Dalton Transactions

ROYAL SOCIETY OF CHEMISTRY

PAPER

View Article Online
View Journal | View Issue

Cite this: *Dalton Trans.*, 2024, **53**, 18193

Thermally stable C_2-symmetric α-diimine nickel precatalysts for ethylene polymerization: semicrystalline to amorphous PE with high tensile and elastic properties†

Xiaoxu Li,‡[a] Zexu Hu,‡[a] Qaiser Mahmood, *[a] Yizhou Wang,[b] Sunny Sohail,[a,b] Song Zou,[b] Tongling Liang [b] and Wen-Hua Sun *[a,b]

Received 6th September 2024,
Accepted 17th October 2024

DOI: 10.1039/d4dt02543a

rsc.li/dalton

In α-diimine nickel catalyst-mediated ethylene polymerization, adjusting catalytic parameters such as steric and electronic factors, as well as spectator ligands, offers an intriguing approach for tailoring the thermal and physical properties of the resulting products. This study explores two sets of C_2-symmetric α-diimine nickel complexes—nickel bromide and nickel chloride—where *ortho*-steric and electronic substituents, as well as nickel halide, were varied to regulate simultaneously chain walking, chain transfer, and the properties of the polymers produced. These complexes were activated *in situ* with Et_2AlCl, resulting in exceptionally high catalytic activities (in the level of 10^6–10^7 g (PE) mol^{-1} (Ni) h^{-1}) under all reaction conditions. Nickel bromide complexes, with higher *ortho*-steric hindrance, exhibited superior catalytic activity compared to their less hindered counterparts, whereas the reverse was observed for complexes containing chloride. Increased steric hindrance in both sets of complexes facilitated higher polymer molecular weights and promoted chain walking reactions at lower reaction temperature (40 °C), while the effect became less pronounced at higher temperature (100 °C). However, the electron-withdrawing effect of *ortho*-substituents hindered the rate of monomer insertion, chain propagation, and chain walking reactions, leading to the synthesis of semi-crystalline polyethylene with an exceptionally high melt temperature of 134.6 °C and a high crystallinity of up to 31.9%. Most importantly, nickel bromide complexes demonstrated significantly higher activity compared to their chloride counterparts, while the latter yielded polymers with higher molecular weights and increased melt temperatures. These high molecular weights, coupled with controlled branching degrees, resulted in polyethylenes with excellent tensile strength (up to 13.9 MPa) and excellent elastic properties (up to 81%), making them suitable for a broad range of applications.

Introduction

Ethylene-α-olefin copolymers, often referred to as polyolefin elastomers (POEs), combine the conventional traits of elastomers with the versatile properties of thermoplastics.[1,2] Due to these qualities, these materials have garnered significant attention and are widely used in automotive components, construction, adhesives, agriculture and electronics.[2] The industrial production of these materials involves copolymerization of ethylene with higher α-olefins using early transition metal catalysts.[3,4] The content, degree, and distribution of branches directly affect their tensile and elastic properties. However, achieving precise control over the microstructure and statistical distribution of comonomers remains a significant challenge in the copolymerization process.[4–6] In recent years, significant academic interest has centered on the nickel-catalyzed preparation of polyethylene elastomers (PEE) using chain-walking mechanisms and ethylene as the only feedstock in polymerization.[7–10]

The well-controlled PEE synthesis can show similar mechanical and elastic properties to POE, along with additional benefits of the easy process of polymerization with the use of one type of monomer, facile synthesis and handling of precatalysts, and excluding the use of expensive comonomers.[1,11,12] The synthesis of PEE under industrially

[a]*Chemistry and Chemical Engineering Guangdong Laboratory, Shantou, 515031, China. E-mail: qaiser@ccelab.com.cn*
[b]*Key Laboratory of Engineering Plastics, Institute of Chemistry, Chinese Academy of Sciences, Beijing, 100190, China. E-mail: whsun@iccas.ac.cn*

†Electronic supplementary information (ESI) available. CCDC 2378621 (**NiBr-iPr**) and 2378622 (**NiBr-Cl**). For ESI and crystallographic data in CIF or other electronic format see DOI: https://doi.org/10.1039/d4dt02543a

‡These authors contributed equally.

relevant conditions typically requires polymerization at high reaction temperatures.[7,10a] However, α-diimine nickel complexes are sensitive to the reaction temperature. They demonstrate low activity, poor polymer molecular weights and less attractive mechanical and elastic properties under industrially relevant conditions, especially, at high polymerization temperatures.[13–15] To address this, in recent years, various types of α-diimine nickel complexes have been reported that demonstrated exceptional catalytic performance for the synthesis of PEE (Chart 1).[11,12,16–32] For instance, unsymmetrical α-diimine nickel precatalysts bearing benzhydryl steric substituents (**I–III**, Chart 1) effectively enabled the synthesis of PEE with high to ultra-high molecular weights and impressive mechanical properties, including notable tensile strength (σ_b = up to 24.5 MPa with an SR value of 58%) and elasticity (up to SR = 87% with σ_b = 3.3 MPa).[11,16,17] The variants featuring fluorinated benzhydryl steric substituents (**IV–VI**, Chart 1) were distinguished by their exceptional thermal stability and capacity to yield PEE with high tensile and elastic characteristics (achieving max. σ_b = up to 21.7 MPa and SR = up to 85%).[18–20] Meanwhile, symmetrical analogues (**VII**, Chart 1) exhibited high activity under industrially relevant conditions (activity up to 2.77 × 10^6 g (PE) mol^{-1} (Ni) h^{-1} at 100 °C) and produced branched PE with ultra-high molecular weight and robust mechanical properties (σ_b = up to 25.9 MPa and SR = up to 62%).[21] Most importantly, the C_2-symmetric variants (**VIII–X**, Chart 1) demonstrated unprecedented catalytic performance, including thermal stability up to 110 °C (1.8 × 10^6 g (PE) mol^{-1} (Ni) h^{-1}), polymer molecular weights ranging from 10^5 to 10^6 g mol^{-1}, and an excellent combination of tensile and elastic features within the same PE sample (σ_b up to 25.9 MPa associated with an SR value of 70%).[22–24] The precatalyst **XI** produced PEE with an elastic recovery of up to 83% and tensile strength in the range of 3 to 28 MPa.[12] Even nickel complexes bearing flexible alkyl *ortho* substituents (**XII**, Chart 1) were highly active in PEE synthesis, achieving excellent elastic recovery (SR = up to 88%, σ_b = 2.0–11.6 MPa).[25] Moreover, the sandwich-like nickel complexes bearing 5-dibenzosuberyl (10,11-dihydro-5*H*-dibenzo[*a*,*d*]cyclohepten-5-yl) and polyethylene glycol substituents (**XIII–XIV**, Chart 1) provided a means to tune the branching and living character of the catalyst with distinct catalytic activities for the synthesis of PEE with tunable tensile and elastic properties (SR = up to 76%, σ_b = 3.0–26.6 MPa).[26,27] These structural advancements highlight the effective catalytic behavior of α-diimine nickel complexes in synthesizing PEE with tunable tensile and elastic properties. Inspired by the thermal stability of **IV–VI** and the mechanical/elastic properties of **VIII–X** catalysts, we have successfully developed a novel series of C_2-symmetric nickel catalysts with the incorporation of fluorine (F) functionalized benzhydryl as

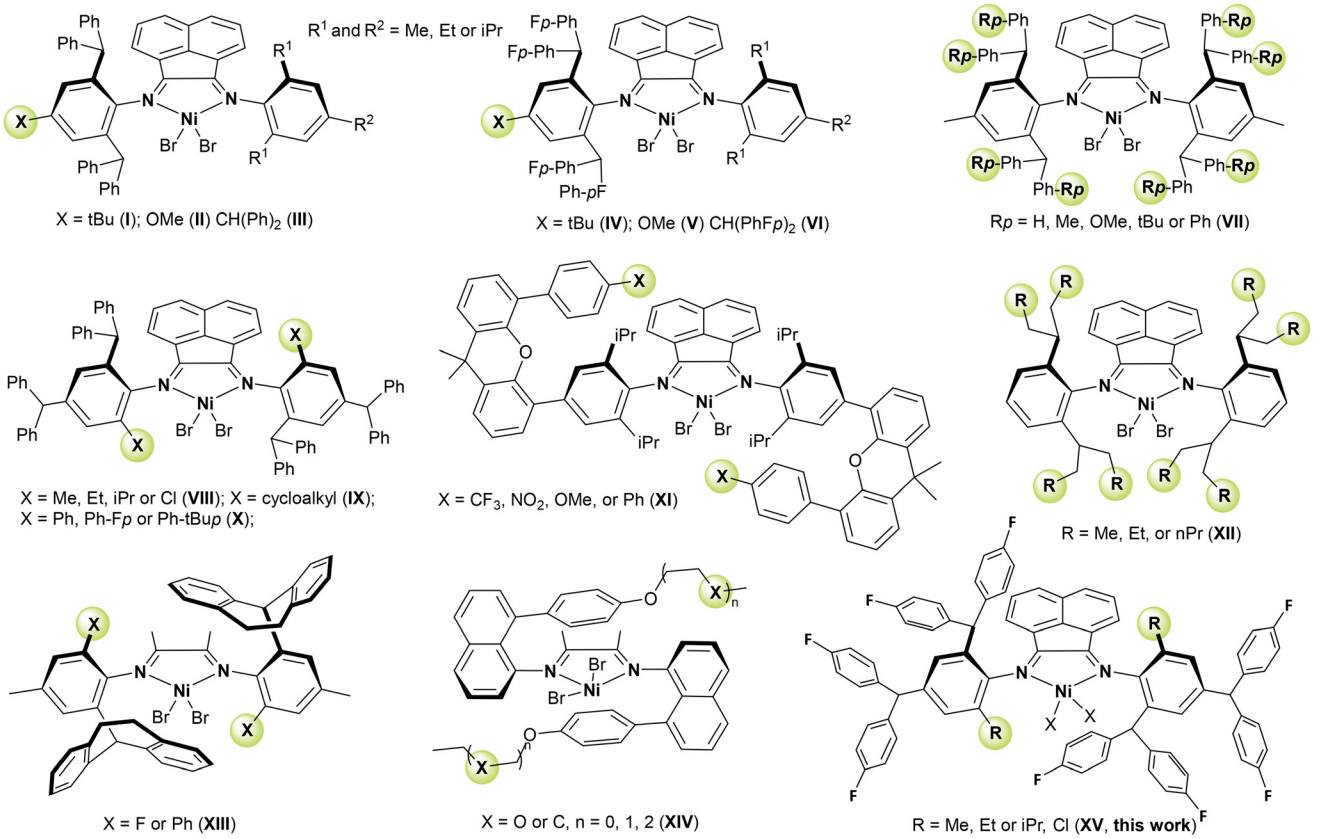

Chart 1 The previously reported representative α-diimine nickel complexes having excellent capabilities to produce PEE along with our current work.

the steric component (**XV**, Chart 1). These catalysts exhibit high catalytic activity, excellent thermal stability, and the ability to tune the polymer molecular weight and branching degree for synthesizing thermoplastic polyethylene elastomers. The resulting PEE demonstrate excellent mechanical and elastic properties, making them suitable for a wide range of applications.

Results and discussion

Synthesis and characterization of ligands and the corresponding nickel complexes

A two-step method was used for the synthesis of these ligands (Scheme 1).[22,23,29] In the first step, the reaction of acenaphthoquinone and the corresponding 2,4-bis(bis(4-fluorophenyl) methyl)-6-alkylaniline at the boiling temperature of the solvent (glacial acetic acid) in the presence of zinc chloride led to intermediate products, and these were identified as zinc complexes in previous reports. In the following step, zinc chloride was removed from the intermediate product in the presence of potassium oxalate in a water/dichloromethane solution, affording the corresponding set of ligands in excellent yields (77%–87%). The non-symmetrical ligand, **L-iPr$_3$**, was prepared under different reaction conditions following our previously reported method (Scheme 1).[11] The condensation reaction of acenaphthoquinone and 2,4-bis(bis(4-fluorophenyl)methyl)-6-isopropylaniline at room temperature in a dichloromethane/ethanol solution afforded the imino-ketone (**3**) in a good yield, and following condensation with 2,6-isopropylaniline produced the ligand, **L-iPr$_3$** (see the ESI† for details). Two sets of complexes, nickel bromides (**NiBr-Me**, **NiBr-Et**, **NiBr-iPr**, **NiBr-Cl**, **NiBr-iPr$_3$**), and chlorides (**NiCl-Me**, **NiCl-Et**, **NiCl-iPr**, **NiCl-Cl**), were obtained in excellent yields by the treatment of symmetrical/non-symmetrical ligands with $NiBr_2$(DME) and $NiCl_2{\cdot}6H_2O$ in ethanol and/or dichloromethane, respectively, at room temperature under an inert atmosphere (Scheme 1). The $^1H/^{13}C$ NMR spectra of the ligands confirmed their C_2 symmetric structures.[33] FTIR spectroscopy revealed imine functional groups with stretching frequencies in the range of 1658–1679 cm^{-1}. In nickel complexes, these frequencies slightly shifted to a lower range of 1627–1660 cm^{-1}, indicating effective coordination between imine and nickel centers. Similar shifting of the stretching frequency of imine has been reported in previous studies.[22,23] The purity of the compounds was confirmed from the carbon, hydrogen, and nitrogen elemental analysis of ligands and complexes and further confirmed from high resolution mass spectroscopy (see Fig. S77–S90 in the ESI†). Moreover, X-ray single crystal diffraction analysis of the selected complexes **NiBr-iPr** and **NiBr-Cl** confirmed tetra-coordinated structures with nickel occupying the central position (Fig. 1 and 2). These structures exhibit some deviation from the regular tetrahedral geometry, consistent with the previously reported nickel complexes bearing the acenaphthoquinone ligand framework. The comparison of bond distances and angles in both imine units are similar.[33] The coordination between the N_{imine} bond and the central nickel atom forms a chelating ring, with a bite angle of 121.492° for **NiBr-iPr** and 128.41° for **NiBr-Cl**. In structures of both complexes, the chelating ring and the backbone of acenaphthoquinone are in one plane, while the plane of the phenyl ring of aniline is almost perpendicular to the plane of the chelate ring. Moreover, the backbone of acenaphthoquinone is sandwiched between the two phenyl rings of benzahydryl groups, possibly due to non-covalent interactions within these groups. Intra ligand non-covalent interactions in the ligand backbone and *ortho* substituents of the *N*-aryl unit, previously reported by Brookhart, Gao, Dai, and others—along with our recent findings—support this observation.[34] These structural features are particularly important to restrict the chain transfer reactions rela-

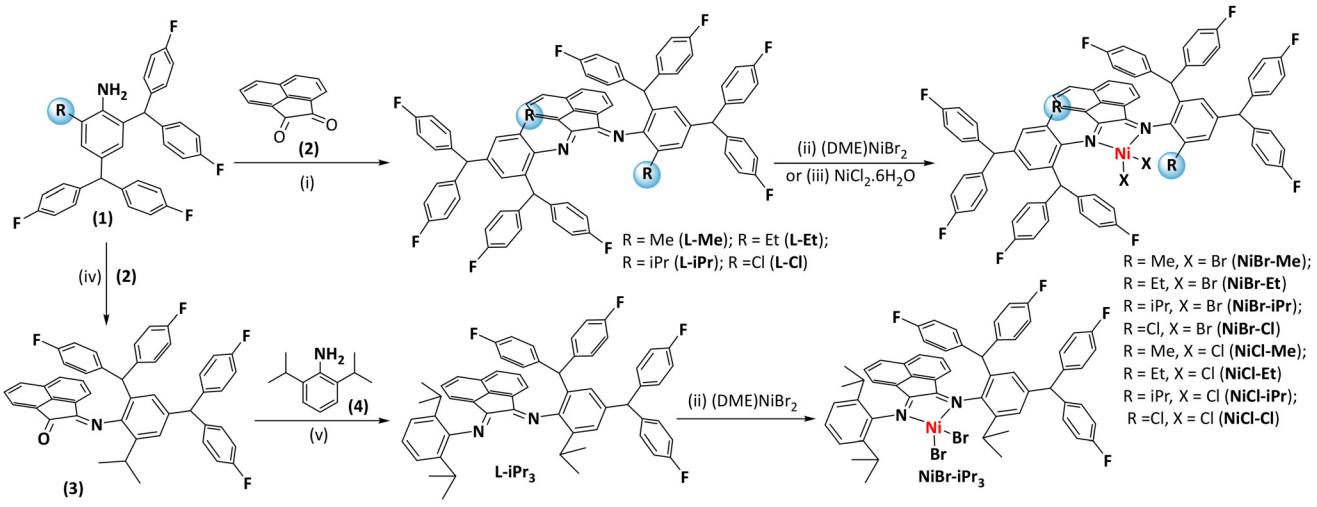

Scheme 1 General synthetic route of symmetrical ligands and their nickel complexes. Conditions: (i) first step: $ZnCl_2$, glacial acetic acid, reflux, 6 h; second step: potassium oxalate, water, dichloromethane, r. t., stirring, 1 h; (ii) dichloromethane, r. t., stirring, 24 h; (iii) ethanol/dichloromethane, r. t., stirring, 24 h; (iv) *p*-TsOH, ethanol/dichloromethane, r. t., stirring, 24 h; (v) *p*-TsOH, toluene, reflux, stirring, 12 h.

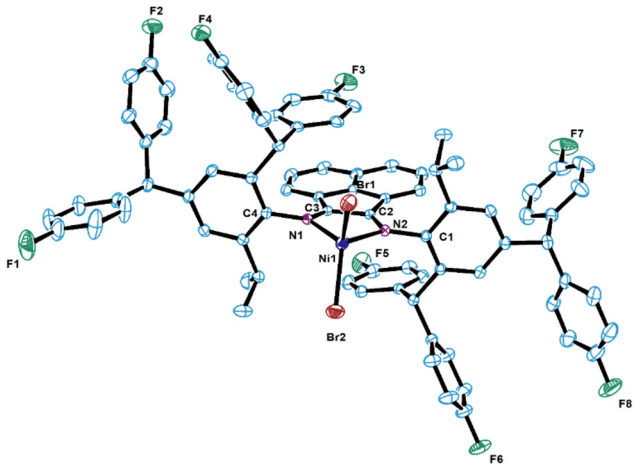

Fig. 1 ORTEP drawing of **NiBr-iPr**. For clarity, all hydrogen atoms and one ether molecule are omitted. Selected bond lengths (Å): Ni1–Br1 2.3413(4), Ni1–Br2 2.3383(4), Ni1–N1 2.0415(14), Ni1–N2 2.0453(13), N1–C3 1.285(2), N1–C4 1.4472(19), N2–C1 1.4486(19), N2–C2 1.286(2) and angles (°): Br2–Ni1–Br1 121.492(15), N2–Ni1–N1 82.74(5), N1–Ni1–Br1 113.55(4), N1–Ni1–Br2 112.36(4), N2–Ni1–Br1 111.36(4), N2–Ni1–Br2 108.55(4).

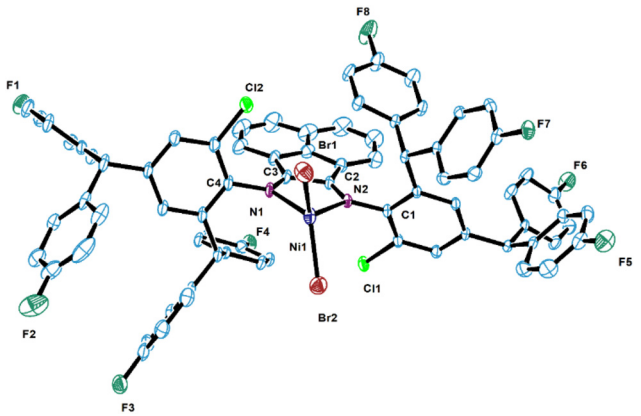

Fig. 2 ORTEP drawing of **NiBr-Cl**. For clarity, all hydrogen atoms and one *n*-hexane molecule are omitted. Selected bond lengths (Å): Ni1–Br1 2.3455(8), Ni1–Br2 2.3336(9), Ni1–N1 2.041(3), Ni1–N2 2.025(3), N1–C3 1.283(6), N1–C4 1.439(4), N2–C1 1.422(4), N2–C2 1.283(5) and angles (°): Br2–Ni1–Br1 128.41(4), N2–Ni1–N1 82.62(14), N1–Ni1–Br1 99.13(9), N1–Ni1–Br2 120.34(10), N2–Ni1–Br1 118.55(9), N2–Ni1–Br2 99.52(9).

tive to the chain propagation, and also beneficial for improving the thermal stability of the precatalysts.[21,34–37]

Ethylene polymerization

Optimization of the cocatalyst and the Al/Ni ratio. First, the reaction conditions were screened to examine the catalytic scope of the prepared catalysts for polymerization of ethylene. The units, g (PE) mol^{-1} (Ni) h^{-1} and g mol^{-1}, used for the activity and polymer molecular weight are not given in the following text to present a simple and easy discussion.

In order to explore the best alkyl aluminum activator for the **NiBr-iPr** precatalyst, four alkyl aluminum co-catalysts—diethyl aluminum chloride (DEAC), methylaluminoxane (MAO), dimethyl aluminum chloride (DMAC), and modified methylaluminoxane (MMAO)—were tested for ethylene polymerization. The polymerization results are presented in Table 1 (entries 1–4). As seen in Fig. 3a, **NiBr-iPr**, activated with 400 equiv. of DEAC or DMAC, exhibited a higher activity compared to MAO and MMAO. However, the latter cocatalysts resulted in polyethylenes with relatively higher molecular weights (entries 1–4, Table 1). The highest activity recorded with DEAC was 11.6×10^6 (entry 4, Table 1). This difference in catalytic performance may stem from the relatively stronger Lewis acidity of DEAC and DMAC, facilitating the rapid activation of the nickel center, while larger counter ions in the case of MAO or MMAO possibly slow down the chain transfer reaction relative to chain propagation, thus resulting in higher molecular weight polyethylene.[38–41] The resulting polymer exhibited a molecular weight at the level of 10^5 g mol^{-1} and a narrow mass distribution (M_w/M_n = 1.48–1.80). Based on the comparison of catalytic activities among different co-catalysts, DEAC was selected as the best co-catalyst for further investigations.

The **NiBr-iPr** catalyst showed significant differences in activities and polymer molecular weights with changes in DEAC amounts (entries 4–8, Table 1). High activities were achieved across all cocatalyst concentrations. According to Fig. 3b, the peak activity was observed at 400 equiv. and activities at 200 and 300 equiv. decreased by factors of 3.1 and 2.0,

Table 1 Selection of the best cocatalyst and amount of co-catalyst for ethylene polymerization using **NiBr-iPr** as the precatalyst[a]

Entry	Cocat.	Al/Ni	Yield (g)	Act[b]	M_w[c]	M_w/M_n[c]	T_m[d] (°C)
1	MAO	2000	7.8	7.8	6.3	1.48	84.3
2	MMAO	2000	7.8	7.8	5.8	1.80	82.3
3	DMAC	400	10.7	10.7	5.0	1.77	80.6
4	DEAC	400	11.6	11.6	3.3	1.75	91.9
5	DEAC	200	3.7	3.7	7.8	1.71	69.4
6	DEAC	300	5.8	5.8	4.1	1.76	94.4
7	DEAC	500	10.7	10.7	3.0	1.53	82.3
8	DEAC	600	6.9	6.9	2.2	1.76	96.2

[a] Conditions: **NiBr-iPr** (2.0 μmol); solvent toluene (100 mL); ethylene (10 atm); reaction time (30 min); temperature (30 °C). [b] Activity unit is given in 10^6 g (PE) mol^{-1} (Ni) h^{-1}. [c] Determined by DSC. [d] Determined by GPC, unit: 10^5 g mol^{-1}.

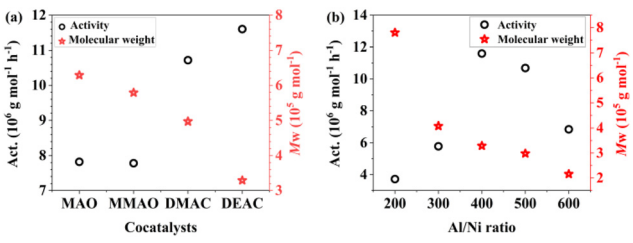

Fig. 3 Activity and polymer molecular weight relationship with (a) the cocatalyst type (entries 1–4, Table 1) and (b) the amount of DEAC (entries 4–8, Table 1).

respectively (entries 5 & 6, Table 1). The activity slightly decreased with an increase in the cocatalyst to 500 equiv., but there was a significant drop at 600 equiv. (entry 7, Table 1). Unlike the catalytic activity, the polymer molecular weight (M_w) gradually decreased with the increase of cocatalyst concentration. There was a significant decrease in the M_w value as the Al/Ni ratio increased from 200 to 300: the M_w value dropped from 7.80×10^5 to nearly half (entry 1, Table 3). Further increase of the cocatalyst concentration led to a consistent decrease in the M_w value, reaching its lowest value of 2.16×10^5 at an Al/Ni ratio of 600 (entry 8, Table 1). A higher concentration of the cocatalyst tends to facilitate chain transfer reactions over chain propagation, which in turn leads to a decrease in the M_w value at elevated cocatalyst concentrations.[10,42–44] Overall, the molecular weight remained high in the range of 10^5 g mol^{-1} across all concentrations of the cocatalyst, with a narrow dispersity (Fig. 3b). The M_w dispersity remained narrow and less affected, highlighting the single-site catalytic behavior of **NiBr-iPr** across all concentrations of the cocatalyst.

Screening of ligand frameworks and halide ligands

To examine the steric and electronic impact of *ortho*-substituents of ligands, all nickel bromide complexes (**NiBr-Me**, **NiBr-Et**, **NiBr-iPr**, **NiBr-Cl**) were tested under similar conditions and compared with their chloride counterparts (**NiCl-Me**, **NiCl-Et**, **NiCl-iPr**, **NiCl-Cl**) and the unsymmetrical analogue (**NiBr-iPr$_3$**). The polymerization tests performed at 40 °C were used for this comparison (entries 2, 8, 12, 16, 20, 24–27, Table 2). The results showed several trends in the catalytic activity and polymer molecular weight with the change of *ortho*-substituents of aniline as illustrated in Fig. 4a. Catalysts with bulkier *ortho*-substituents exhibited higher activity and produced higher molecular weight polyethylene than those with less steric hindrance.[22,23] For instance, the replacement of the *ortho*-methyl substituent in **NiBr-Me** by the *ortho*-ethyl substituent in **NiBr-Et** increased the catalytic activity by 2% from 10.3×10^6 to 10.5×10^6 and the polymer M_w value increased by 4% from 2.2×10^5 to 2.5×10^5 (entries 8 *vs.* 12). A more significant difference was observed when **NiBr-Et** was replaced by **NiBr-iPr**, resulting in 16% increase in activity and 38% increase in the M_w value (entries 2 *vs.* 8). The activity and polymer M_w decreased in the order: **NiBr-iPr** (R = iPr) > **NiBr-Et** (R = Et) > **NiBr-Me** (R = Me) (entries 2, 8, 12). Moreover, the symmetrical complex **NiBr-iPr** showed a dramatic improvement in the catalytic performance as compared to the unsymmetrical **NiBr-iPr$_3$** complex: 90% increase in the activity from 6.4×10^6 to 12.2×10^6 and 110% increase in the molecular weight from 1.6×10^3 to 3.3×10^3 (entry 2 *vs.* 20). These results can be ascribed to the fact that an increase in the steric hindrance of the *ortho*-substituent increases the rate of chain propagation over the chain transfer reactions and increases the ratio of the insertion transition state relative to the resting state, resulting in higher M_w values and activities,

Table 2 Ethylene polymerization results using different precatalysts at different temperatures[a]

Entry	Cat.	T (°C)	Mass (g)	Act.[b]	M_w[c]	M_w/M_n[c]	T_m[d] (°C)	X_c[d] (%)	BD[e]
1	**NiBr-iPr**	30	11.6	11.6	3.4	2.19	91.9	3.49	35
2	**NiBr-iPr**	40	12.2	12.2	3.3	2.45	94.8	8.07	60
3	**NiBr-iPr**	50	6.9	6.9	2.2	1.87	93.1	3.90	62
4	**NiBr-iPr**	60	6.6	6.6	2.1	1.89	90.8	2.85	65
5	**NiBr-iPr**	70	6.3	6.3	1.9	2.06	—[f]	—[f]	68
6	**NiBr-iPr**	80	5.4	5.4	1.5	1.94	—[f]	—[f]	69
7	**NiBr-iPr**	100	4.8	4.8	1.1	1.89	—[f]	—[f]	76
8	**NiBr-Et**	40	10.5	10.5	2.5	1.80	102.4	0.93	57
9	**NiBr-Et**	60	5.3	5.3	1.8	1.99	73.0	0.36	60
10	**NiBr-Et**	80	2.1	2.1	1.6	1.89	70.6	0.80	61
11	**NiBr-Et**	100	0.8	0.8	1.0	1.93	—[f]	—[f]	66
12	**NiBr-Me**	40	10.3	10.3	2.2	2.08	108.9	14.6	42
13	**NiBr-Me**	60	5.0	5.0	1.7	2.01	81.6	2.02	61
14	**NiBr-Me**	80	2.6	2.6	1.3	2.56	80.4	2.58	66
15	**NiBr-Me**	100	1.7	1.7	1.0	2.15	69.1	1.49	75
16	**NiBr-Cl**	40	6.6	6.6	1.2	1.98	134.6	31.9	41
17	**NiBr-Cl**	60	5.7	5.7	1.0	2.35	104.9	7.77	45
18	**NiBr-Cl**	80	1.5	1.5	0.8	1.89	96.7	5.27	56
19	**NiBr-Cl**	100	1.0	1.0	0.4	1.92	76.7	2.36	61
20	**NiBr-iPr$_3$**	40	6.4	6.4	1.6	2.32	—[f]	—[f]	75
21	**NiBr-iPr$_3$**	60	7.4	7.4	1.4	1.91	—[f]	—[f]	83
22	**NiBr-iPr$_3$**	80	2.9	2.9	1.2	2.37	—[f]	—[f]	88
23	**NiBr-iPr$_3$**	100	2.5	2.5	0.6	1.92	—[f]	—[f]	96
24	**NiCl-iPr**	40	6.4	6.4	6.7	2.06	98.7	2.71	45
25	**NiCl-Et**	40	7.3	7.3	5.2	2.66	92.5	5.36	37
26	**NiCl-Me**	40	7.6	7.6	5.4	1.73	110.2	5.57	33
27	**NiCl-Cl**	40	5.2	5.2	1.7	2.12	124.2	14.5	36

[a] General conditions: precat. (2.0 μmol); cocat. (DEAC); Al/Ni ratio (400); toluene solvent (100 mL); ethylene (1 MPa); reaction time (30 min). [b] Activity unit is given in 10^6 g (PE) mol^{-1} (Ni) h^{-1}. [c] Determined by GPC. [d] Determined by DSC; $X_c = \Delta H_f(T_m)/\Delta H_f^\circ(T_m^\circ)$, $\Delta H_f^\circ(T_m^\circ) = 248.3\,\mathrm{J\,g^{-1}}$. [e] Branches per 1000 carbons, determined by ^{1}H NMR spectra $[(2 \times I_{Me}/3 \times I_{total}) \times 1000]$. [f] No specific melt temperature.

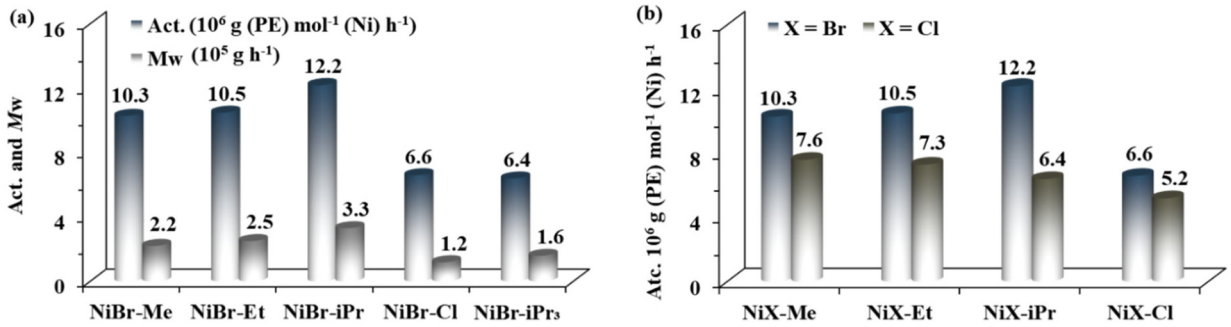

Fig. 4 (a) Activity and polymer molecular weight relationship with the ligand framework (entries 2, 8, 12, 16 and 20 in Table 2); (b) activity relationship with the spectator ligand (entries 2, 8, 12, 16 *vs.* 24–27 in Table 2).

respectively.[31,45–47] Moreover, the M_w dispersity of PE obtained from symmetrical nickel complexes was narrower than that from the unsymmetrical complex. This difference also supports the higher M_w value of polyethylene obtained with symmetrical nickel precatalysts (entries 2, 8 and 12), highlighting the significant role of steric hindrance in improving the catalytic performance for ethylene polymerization (Fig. 4a).

In addition, the electronic effect of the *ortho*-substituent was investigated by comparing precatalysts **NiBr-Me** and **NiBr-Cl** under similar conditions (entries 12 & 16, Fig. 4a). The complex **NiBr-Cl**, bearing an electron-withdrawing *ortho*-substituent (R = Cl), exhibited an activity of 6.6×10^6, which is significantly lower than that of **NiBr-Me**, bearing the electron-donating *ortho*-substituent (R = Me). The M_w of PE followed the same trend as for the activity. Although, the exact reasons for these results remain unclear, it is possible that the electron-donating effects of the methyl group on the metal center contribute to an increased insertion transition state relative to the resting state and an interaction of the Cl unit with β-H on the growing polymer chain could be operative in this system, which can facilitate chain transfer and lead to a lower molecular weight.[48–50] Meanwhile, the presence of the *ortho*-methyl substituent likely increases the solubility of the precatalyst, resulting in higher catalytic activity obtained for **NiBr-Me**.[51]

Change of the auxiliary ligand from Br to Cl showed great influence on the catalytic performance. Among the nickel chloride complexes (**NiCl-Me**, **NiCl-Et**, **NiCl-iPr**), the dependence of catalytic activity upon the *ortho*-substituent followed an opposite trend observed in the set of nickel bromide precatalysts *i.e.*, **NiCl-Me** (R = Me) > **NiCl-Et** (R = Et) > **NiCl-iPr** (R = iPr). These results indicated that the increased steric hindrance of *ortho*-substituents had a negative effect on the catalytic activity (Fig. 4b).[22,52] Likely, more steric hindrance of the *ortho*-substituent facilitate stabilization of resting states relative to the insertion transition states.[45] Although the M_w value of the polyethylene obtained with **NiCl-Me** was roughly similar to that obtained with **NiCl-Et**, the molecular weight of the polyethylene produced from **NiCl-iPr** was comparatively higher than these precatalysts, indicating that more steric hindrance promotes chain propagation reactions rather than chain transfer reactions. This fact is similar to the observation found in the series of nickel bromide precatalysts. Moreover, nickel chloride precatalysts exhibited significantly lower activities when put alongside their bromide counterparts, while this fact was opposite regarding polymer molecular weights (Fig. 4b).[11] For instance, the replacement of bromide (**NiBr-iPr**) with chloride (**NiCl-iPr**) resulted in a decrease of about 50% in the catalytic activity from 12.2×10^6 to 6.4×10^6 and an increase of about 100% in the molecular weight of polyethylene from 3.3 to 6.7 (entries 2 *vs.* 24). An almost similar difference in the activity and M_w value was noted for other nickel bromide (**NiBr-Me**, **NiBr-Et**) and chloride (**NiCl-Me**, **NiCl-Et**) precatalysts. The precise explanation behind these differences in the catalytic performance remains unclear but it may be related to the different activation processes, stability of the active species and resultant counter-ion type.[38–41,53] The M_w distributions in both sets of nickel precatalysts were similar and narrow (M_w/M_n = 1.73–2.66 for nickel chloride precatalysts).

Thermal stability assessment of nickel complexes

The thermal stability of all nickel complexes was assessed at temperatures in the range of 30 to 100 °C under consistent conditions of DEAC (Al/Ni = 400), toluene (100 mL), ethylene at 1 MPa, and a runtime of 30 minutes (Table 2 and Fig. 5a). In the case of **NiBr-iPr**, an initial rise in the temperature from 30 °C to 40 °C showed a slight increase in the catalytic activity, but a further elevation of temperature led to a decrease in the activity, likely due to the partial decomposition of the active species and reduced ethylene solubility.[24,36,37,54–56] Compared to other Ni complexes, the **NiBr-iPr** complex exhibited the highest overall activity and maintained it exceptionally well, reaching 4.8×10^6 even at 100 °C (entry 7, Table 2). This level of activity at elevated temperatures is rare among α-diimine nickel complexes and is attributed to the incorporation of fluorine functionalized benzhydryl as steric *ortho* substituents on the aniline moieties, which restrict the *N*-aryl rotation and prevent C–H activation.[23,35,57] The electron-withdrawing F substituent may facilitate non-covalent interactions between the phenyl cap of the benzhydryl unit and the acenaphthoquinone backbone. The distance between these groups was calculated as 3.449 Å for **NiBr-iPr**, indicating non-covalent interactions. This interaction distinguishes it from other α-diimine nickel

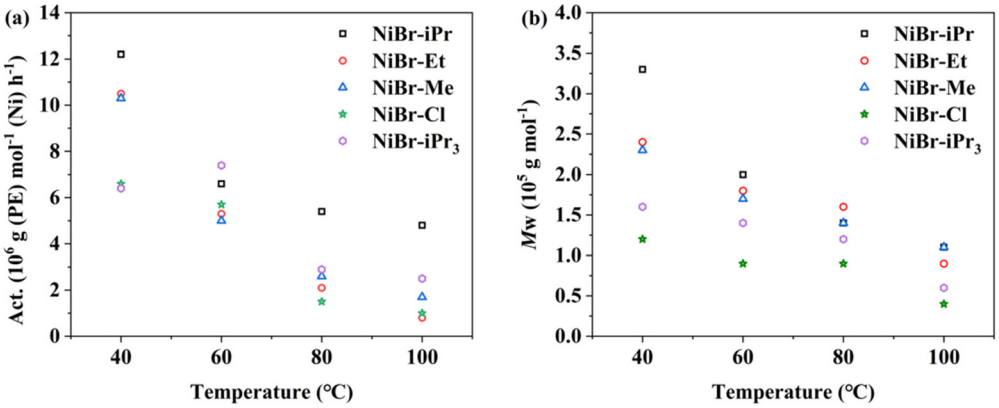

Fig. 5 (a) Changes in the catalytic activity (a) and polymer molecular weights (b) at different polymerization temperatures using different nickel pre-catalysts (entries 2, 4, 6, 7, 8–23 in Table 2).

catalysts containing simple benzhydryl groups.[22] Such non-covalent interactions have a significant impact on the thermal stability of the precatalysts, a phenomenon previously reported in similar systems.[34] In contrast, **NiBr-Me**, while being the second-best in terms of initial activity, showed a sharp decline in the activity from 10.3×10^6 at room temperature to 5.0×10^6 at 60 °C and further dropping to 1.7×10^6 at 100 °C. **NiBr-Et** was the least thermostable, giving an activity of 0.8 at 100 °C (entries 12–15, Table 2). **NiBr-Cl**, with its electron-withdrawing *ortho* substituent, exhibited slightly lower thermal stability than **NiBr-Me** with its electron-donating substituent. The unsymmetrical **NiBr-iPr$_3$** complex, although lower in activity compared to the symmetrical **NiBr-iPr**, showed better thermostability than **NiBr-Me** and **NiBr-Et** across the temperature range tested. The exceptional thermal stability of **NiBr-iPr** is noteworthy and indicates the importance of sterically bulky substituents in enhancing the stability of nickel complexes at elevated temperatures.

Along with the activity, the molecular weights of the obtained polyethylene gradually decreased in all cases (Fig. 5b). For instance, the polymer M_w value for **NiBr-iPr** decreased from 3.3×10^5 at 40 °C to 1.1×10^5 at 100 °C, while maintaining controlled molecular weight dispersity. A more significant decrease in molecular weights was observed for **NiBr-Cl** (M_ws = 1.2×10^5 at 40 °C decreased to 0.4×10^5 at 100 °C), whereas other nickel complexes showed a less pronounced trend. These results suggest that the relative rate of chain transfer to monomer insertion (k_{tr}/k_{ins}) increases with the reaction temperature, leading to lower polymer molecular weights at higher temperatures.[33,58,59] Despite the temperature-induced decrease, polymer molecular weights remained high in the level of 10^5 g mol^{-1} for **NiBr-iPr** and **NiBr-Me** across all reaction temperatures, with narrow M_w distributions ($M_w/M_n < 2$).

Effect of ethylene pressure and reaction time

Through the investigation of ethylene polymerization reactions at different time intervals (entries 1–6, Table 3), it was found that the **NiBr-iPr**/DEAC catalytic system has a relatively short induction period. When the polymerization time was only 5 min, the activity could reach an ultra-high value of 17.16×10^6 (entry 1, Table 3). However, when the reaction time was extended, the activity gradually decreased. This decline is likely due to issues with the polymer mass removal and/or the decomposition of active species.[60–62] Despite the decrease in the rate of polymerization over time, the activity of 7.63×10^6 obtained after 60 min is still considered an excellent value (entry 6, Table 3). This indicates that the maximum active species are formed with the addition of the cocatalyst and remain active for a prolonged reaction time. Moreover, with the exception of the M_w value of polyethylene in entry 4 (Table 3), the molecular weights, as expected, gradually increased with time from 3.57×10^5 to 6.55×10^5. This indicates that chain growth reactions continuously increased over time, resulting in relatively higher molecular weight polyethylene. The gradual decrease in the dispersity value further supports these results and the single-site catalytic behavior of this system.

As expected, the catalytic activity increases linearly with higher ethylene pressure (entries 4, 7–9, Table 3). The activity

Table 3 Ethylene polymerization at varying ethylene pressure and reaction time[a]

Entry	C_2H_4 (MPa)	Time (min)	Yield (g)	Act. (10^6)[b]	M_w (10^5)[c]	M_w/M_n[c]	T_m[d] (°C)
1	1.0	5	2.9	17.1	3.6	1.84	87.3
2	1.0	10	4.4	13.1	4.4	1.81	76.7
3	1.0	20	8.2	12.4	5.0	1.41	75.1
4	1.0	30	12.2	12.2	3.3	1.77	93.1
5	1.0	45	15.2	10.1	5.4	1.35	93.1
6	1.0	60	15.3	7.7	6.6	1.79	85.7
7	0.1	30	2.1	2.1	2.0	1.71	—
8	0.5	30	6.9	6.9	3.3	1.97	82.2
9	2.0	30	19.9	19.9	4.0	1.76	102.4

[a] Conditions: **NiBr-iPr** (2.0 μmol); toluene solvent (100 mL); ethylene (10 atm); reaction time (30 min); temperature (30 °C). [b] Activity unit is given in g (PE) mol^{-1} (Ni) h^{-1}. [c] Determined by DSC. [d] Determined by GPC.

at 0.1 MPa was 2.1×10^6 and significantly increased by approximately 230% at 0.5 MPa, 480% at 1 MPa, and 850% at 2.0 MPa. The rate of polymerization follows first-order reaction kinetics, primarily depending on ethylene concentrations. Prior studies revealed that higher ethylene pressure favors chain growth reactions over chain transfer reactions, leading to a gradual increase in polymer molecular weights.[47,63,64] The highest molecular weight, 4.0×10^5, was achieved at 2 MPa ethylene. Additionally, the polymer melt temperature increased linearly from 82.2 to 102.4 °C with an increase of ethylene pressure. This suggests fewer branches in the resulting polyethylene and a more crystalline microstructure.

Microstructure of polyethylene

The polymer melt temperature and branching degree exhibit a significant relationship with the steric hindrance of *ortho*-substituents and polymerization temperature, and are also interrelated.[12,52,56] The melt temperature was determined from the DSC thermogram, while the branching degree and types of branches were identified from high-temperature ^{1}H and ^{13}C NMR spectra. The DSC thermogram reveals high polymer melt temperatures in the range of 94.8 to 134.6 °C for PEs obtained at a polymerization temperature of 40 °C using nickel bromides (entries 2, 8, 12, and 16, Table 2) and in the range of 92.5 to 124.2 °C for nickel chloride complexes (entries 24–27, Table 2). Interestingly, the polymer melt temperature gradually decreased from 108.9 to 94.8 °C with the increase in the steric bulkiness of *ortho*-substituents from Me to iPr in nickel bromide complexes, and a similar trend was observed in nickel chloride complexes. This tendency suggests a correlation with the branching degree of the obtained PE, where more sterically hindered nickel complexes facilitate more chain walking reactions compared to less hindered counterparts.[23,31,56,65] An exceptionally high melt temperature of 134.6 °C, along with significant crystallinity (31.9%), was achieved for the **NiBr-Cl**-based polyethylene, a result rarely reported in α-diimine nickel-catalysed ethylene polymerization (entry 16, Table 2). Similarly, the **NiCl-Cl**-based polyethylene exhibited a high melt temperature of 124.2 °C (entry 27, Table 2). These high value of melt temperatures underscore the semicrystalline nature of the resulting polyethylene. The wide-angle X-ray diffraction (WAXD) of the **NiBr-Cl**-based PE sample revealed two prominent peaks at 2θ = 21.4° and 23.7°, corresponding to the (110) and (200) lattice planes of the orthorhombic unit cell of polyethylene, confirming the crystalline nature of the obtained polymer (Fig. S76a†). In contrast, polyethylene produced with **NiBr-iPr$_3$** under similar conditions was entirely amorphous, lacking a discernible melt temperature. The WAXD spectra of this sample further support its amorphous nature, showing no distinct peaks, unlike those observed for the **NiBr-Cl**-based polyethylene (Fig. S76b†). This difference is likely due to the branching density of the resulting polyethylene. As shown in Fig. 6, the **NiBr-iPr** based PE exhibits a higher branching degree (BD = 60/1000 C) with a lower melt temperature (T_m = 94.8 °C) compared to that observed for **NiBr-Me** (BD = 42/1000 C, T_m = 108.9 °C), a

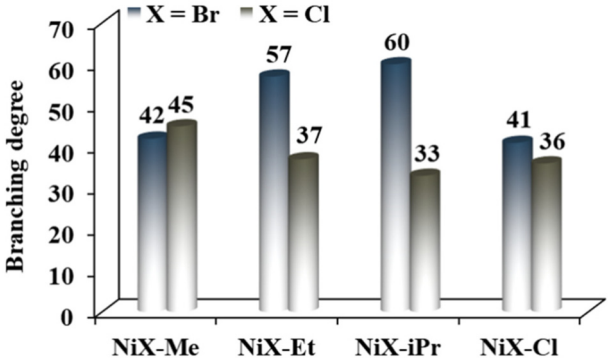

Fig. 6 Branching degree of the PE obtained using different nickel bromide and nickel chloride complexes (entries 2, 8, 12, 16 *vs.* 24–27 in Table 2).

further lower branching density for **NiBr-Cl** (41/1000 C). On the other hand, **NiBr-iPr$_3$** exhibited a much higher branching degree under similar conditions (75/1000 C). A similar relationship between the branching degree and the melt temperature with *ortho*-substituents was also noted in nickel chloride complexes. Considering these results, the *ortho*-Cl group may be involved in the interaction with β-H on the growing polymer chain, which restricts the chain walking reactions, resulting in semi-crystalline PE with a higher melt temperature and less branching. A similar effect was noted for **NiCl-Cl** *versus* **NiCl-R** (R = Et or iPr). These results underscore the significant influence of steric and electronic effects on chain walking reactions and consequently on polymer properties.

Moreover, the polymer melt temperature gradually decreases with the increase of the polymerization temperature, a fact observed in previous studies.[11,12,16] For instance, in **NiBr-iPr**-mediated ethylene polymerization, the melt temperature decreased from 94.8 °C to 90.8 °C as the polymerization temperature was raised from 40 °C to 60 °C (entries 2–4, Table 2). Above this temperature range, no distinct melt temperature was observed, indicating the formation of a completely amorphous polymer (entries 2–7, Table 2). Similar trends were observed with other nickel complexes used in ethylene polymerization. Meanwhile, **NiBr-iPr$_3$** produced polyethylene that was entirely amorphous without a discernible melt temperature across all polymerization temperatures. It is widely accepted that at higher temperatures, chain walking reactions accelerate due to reduced energy barriers for β-agostic alkyl metal complex formation.[45,56,65] The branching degree gradually increased with rising reaction temperatures. For example, the branching degree for **NiBr-iPr** was 35/1000 C at 30 °C, which increased to 76/1000 C at 100 °C, representing an increase of approximately 120% (entries 1–7, Table 2). A similar trend was observed for other nickel complexes. Therefore, the microstructure of the resulting PE gradually shifts from semi-crystalline to fully amorphous. The unsymmetrical nickel complex **NiBr-iPr$_3$** based PE exhibited much higher number of branching which increased from 75/1000 C at 40 °C to 96/1000 C at 100 °C with no specific melt tempera-

ture across all reaction temperatures (Table 2, entries 20–23). To delve deeper into the nature and composition of these branches, high-temperature ^{13}C NMR analysis was conducted on the PE obtained with **NiBr-iPr** at 40 °C and 100 °C, and the results are presented in Fig. 7 and Fig. S38,† respectively. At 40 °C, the obtained PE exhibited a branching degree of 60/1000 C, comprising C_1 (73%), C_2 (4%), C_3 (4%), and C_{4+} (19%). Increasing the polymerization temperature to 100 °C raised the branching degree to 76/1000 C, with C_1 (59%), C_2 (10%), C_3 (6%), and C_{4+} (25%). As anticipated, higher temperatures led to a decrease in short branches from 73% to 59%, along with an increase in longer branches from 19% to 25%. These longer branches contribute to the increasing amorphous character of polyethylene, determined by the absence of specific melt temperatures.

Mechanical and elastic properties

The polymerization temperature significantly influences the microstructure of the resulting polyethylenes (*vide supra*), which in turn defines their physical properties.[1,11,12] To investigate these properties, selected samples prepared at different polymerization temperatures using the **NiBr-iPr**/DEAC catalytic system were tested for stress–strain and elastic measurements

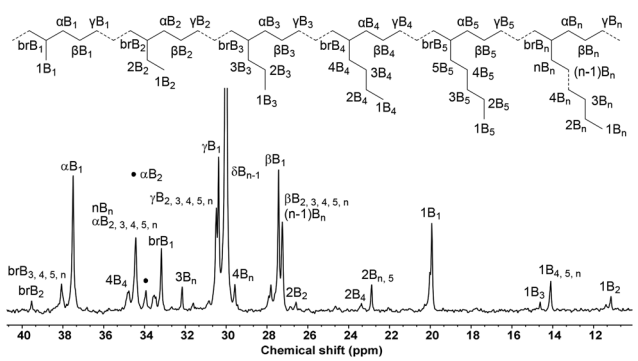

Fig. 7 The high temperature ^{13}C NMR spectrum of **NiBr-iPr**/DEAC mediated ethylene polymerization at 100 °C (entry 7, Table 2).

(entries 2, 4, 6 and 7 in Table 2). The obtained stress–strain curves and hysteresis experiments of strain recovery are shown in Fig. 8. The tensile strength (σ_b) varies from 13.9 MPa to 5.9 MPa, with the associated strain at break (ε_b) falling in the range of 1373.7% to 4993.7% (Fig. 8a). It is found that the tensile strength gradually dropped, while the associated tensile strain increased with the increase of branching degree of the obtained polyethylene. The branching degree is greatly linked to the reaction temperature. Prior studies indicate that polyethylene with fewer branches is more crystalline, while a higher branching degree with longer branches makes it amorphous.[9,22] Thus, the polyethylene prepared at 40 °C (BD = 60/1000 C, M_w = 3.3 × 10^5) exhibited an ultimate tensile strength of 13.9 MPa and an associated strain at a break of 1373.7%. In contrast, the polyethylene obtained at 100 °C (BD = 76/1000 C, M_w = 1.1 × 10^5) showed significantly lower tensile strength and higher tensile strain: σ_b = 5.9 MPa; ε_b = 4993.7%.

Under a fixed strain of 300%, strain recovery hysteresis experiments up to 10 cycles were conducted for the same samples. The strain recovery (SR) varied from 53% to 81% and was greatly linked with the branching degree. As shown in Fig. 8b, the SR value gradually increased with the rise in polymerization temperature and higher branching degree at elevated temperatures. At 40 °C, the resulting polyethylene had the lowest SR value of 53%, which improved approximately linearly to 64%, then to 68%, and finally to an excellent value of 81% with the rise in reaction temperature to 60 °C (BD = 65/1000 C), 80 °C (BD = 69/1000 C), and 100 °C (BD = 76/1000 C), respectively. In general, polyethylenes prepared at 100 °C demonstrated superior elastic properties compared to the polyolefin studied by Ricci *et al.*[47] Their SR values are comparable to or slightly lower than those reported by Coates *et al.* for multiblock copolymers[66] and are equivalent to those of the olefin block copolymers commercialized by Dow.[67] Additionally, similar SR values have been observed in previously reported symmetrical α-diimine nickel precatalyst-based polyethylenes.[11,12,16–18] Prior studies revealed that the elastic properties of the polyolefin arise from their multiblock microstructure,

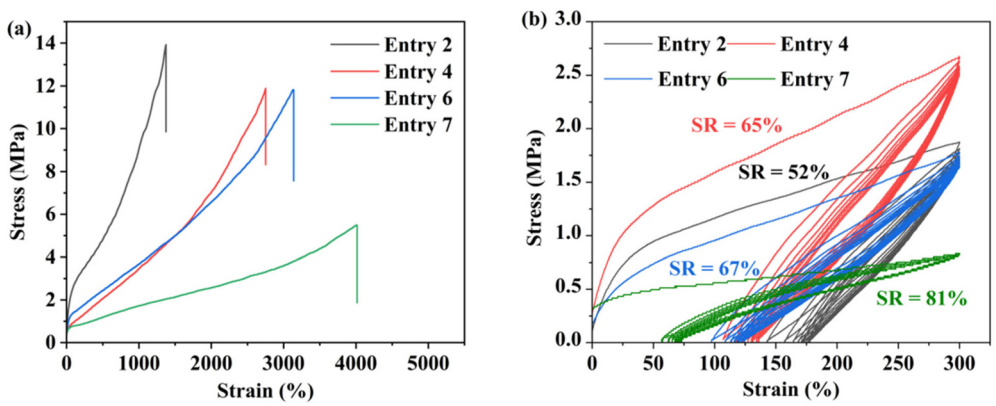

Fig. 8 (a) Tensile strength and (b) strain recovery behavior of polyethylene obtained at different polymerization temperatures using the **NiBr-iPr**/DEAC catalytic system (entries 2, 4, 6, and 7 in Table 2).

having both hard and soft segments.[68] Changes in the catalyst geometry with changes in reaction conditions can generate a multiblock-type polyolefin. The exact reasons are not clear, but we assume that the C_2 symmetric structure of the prepared nickel complexes may adopt different isomeric structures due to differences at the *ortho* position of aniline, resulting in different steric hindrance on the active species. This is more likely to happen at higher temperatures, which makes the rotation of *N*-aryl groups easier. Thus, it may give rise to the formation of a multiblock polymer with both soft and hard segments. This is supported by the ^{13}C NMR measurements revealing diverse compositions of branches along the polymer chain.

Comparison with previously reported α-diimine nickel precatalysts

For comparison, the catalytic performance of the prepared nickel precatalysts was evaluated alongside previously reported catalysts with varying ligand structures (**I–XV**, Chart 1). For instance, the benzhydryl and fluorinated-benzhydryl unsymmetrical α-diimine nickel precatalysts (**I–VI**, Chart 1) exhibited high catalytic activity and thermal stability (up to 90 °C), producing PEE with high to ultra-high molecular weights and remarkable elastic properties (SR up to 87%).[11,16–20] The resulting polyethylene displayed an ultra-high branching degree (up to 200/1000 C) and moderate melting points, depending on the reaction conditions. The symmetrical analogues (**VII**, Chart 1) displayed relatively higher thermal stability (as high as 2.77×10^6 g (PE) mol^{-1} (Ni) h^{-1} at 100 °C) and produced PEE with moderate branching (26–71/1000 C), ultra-high molecular weights, excellent tensile strength (up to 25.9 MPa), and moderate elastic recovery (up to 62%).[21] The polymer melt temperatures were typically around 60 °C in most cases. In comparison, the C_2-symmetric variants (**VIII–X**, Chart 1) showed further higher activity, thermal stability, and polymer properties.[22–24] In particular, precatalyst **IX** exhibited an outstanding combination of tensile strength and elasticity within the same PE sample (tensile strength up to 25.9 MPa with a SR value of 70%), while precatalyst **VIII** bearing *ortho* electron-withdrawing Cl substituents produced polyethylene with high melt temperatures, ranging near 100 °C and reaching a maximum of 130 °C. Precatalyst **XI**, featuring electron-withdrawing groups, produced polyethylene with a higher melt temperature (above 100 °C) and a lower degree of branching (28–41 branches per 1000 carbons at 20 °C).[12] In contrast, its electron-donating counterpart generated polyethylene with a lower melt temperature (around 40 °C) and a higher branching degree (61–78 branches per 1000 carbons at 20 °C).[12] This difference is likely due to the interaction of electron-withdrawing groups (*e.g.*, NO_2 and CF_3) with β-H on the growing polymer chain, reducing the branching and thus increasing the melt temperature. A similar trend was observed with precatalyst **XIII** (Chart 1), where *ortho*-electron withdrawing groups led to polyethylene with a low branching degree and high melt temperature.[26] Comparable properties were also observed in ethylene polymerization mediated by precatalyst **XIV** (Chart 1).[27] However, this phenomenon was not seen in precatalyst **XII**, which features flexible *ortho* substituents that produced polyethylene with a lower melt temperature, higher branching, and excellent elastic properties (SR up to 88%).[25] In comparison, the precatalysts developed in this work had a significant impact on the catalytic performance, particularly in terms of thermal stability (activity: 4.8×10^6 g (PE) mol^{-1} (Ni) h^{-1} at 100 °C), branching degree (low to moderate) and melt temperature. The resulting polyethylene exhibited a high melt temperature, near 100 °C, with an exceptionally high value of 134.6 °C and notable crystallinity (31.9%) for the precatalyst bearing an *ortho* electron-withdrawing group. Additionally, the polyethylene exhibited excellent mechanical properties, including a tensile strength of up to 13.9 MPa, a maximum strain at a break of 1373.7%, and strain recovery up to 81%. Similar to precatalysts **VIII**, **XI** and **XIII** (Chart 1), the high melt temperature is likely due to the interaction of electron-withdrawing groups with β-H on the growing polymer chain, reducing the branching and increasing the melt temperature. Moreover, the fluorine-functionalized benzhydryl groups, acting as sterically hindered *ortho* substituents on the aniline moieties, likely promote non-covalent interactions between the phenyl cap of the benzhydryl unit and the acenaphthoquinone backbone. This interaction sets it apart from other α-diimine nickel catalysts containing simple benzhydryl groups.[22] Such non-covalent interactions play a crucial role in enhancing the thermal stability of the precatalysts, a behavior that has been previously observed in similar systems.[34] These findings demonstrate the effectiveness of these complexes in controlling chain-walking reactions, producing polyethylene with exceptional thermal and mechanical properties, ranging from amorphous to semicrystalline forms.

Experimental section

Synthesis of ligand

Synthesis of L-Me. Acenaphthenequinone, **2** (0.48 g, 2.64 mmol) and $ZnCl_2$ (0.41 g, 3 mmol) were added to a 100 mL flask, followed by the addition of 30 mL of acetic acid. A calculated amount of 2,4-bis(bis(4-fluorophenyl)methyl)-6-methylaniline, **1** (3.7 g, 7.13 mmol), was then added, and the mixture was refluxed at 140 °C for 6 hours. After cooling, the mixture was filtered and washed with acetic acid 4–5 times. Subsequently, 100 mL of n-hexane was added, stirred for 10 minutes, washed 3–4 times, filtered, and dried. The resulting reaction product (2.7 g, 2.1 mmol) was dissolved in 20 mL of dichloromethane and mixed with 20 mL of water containing potassium oxalate (0.78 g, 4.2 mmol), and stirred for 2 hours. After washing with water twice, Na_2SO_4 was added. Most of the solvent was removed using a vacuum pump, and the product was recrystallized with dichloromethane to obtain a yellow powder (2.45 g, 86%). ^1H NMR (400 MHz, chloroform-d): δ 7.76 (d, J = 8.2 Hz, 2H), 7.14 (dd, J = 8.3, 7.2 Hz, 2H), 7.07–6.96 (m, 18H), 6.82 (d, J = 7.0 Hz, 8H), 6.67–6.64 (m, 4H), 6.45 (d, J = 1.9 Hz, 2H), 6.28 (d, J = 7.1 Hz, 2H), 5.97 (t, J = 8.6 Hz, 4H),

5.59 (s, 2H), 5.47 (s, 2H), 2.22 (s, 6H). ^{13}C NMR (101 MHz, chloroform-d): δ 147.3, 140.0, 131.0, 130.7, 130.6, 130.6, 129.0, 128.7, 125.4, 54.7, 50.9, 18.0. FTIR (KBr, cm^{-1}): 714 (w), 778 (m), 828 (s), 927 (w), 1015 (w), 1095 (w), 1156 (m), 1224 (s), 1440 (w), 1467 (w), 1505 (s), 1599 (m), 1660 (ν(C=N), w), 3049 (w). Anal. calcd for $C_{78}H_{52}F_8N_2$ (1169.28): C, 80.12; H, 4.48; N, 2.40. Found: C, 79.98; H, 4.59; N, 2.41. MS-ESI (*m*/*z*): calcd for $[(C_{78}H_{52}F_8N_2) + H]^+$: 1169.40755. Found: 1169.40674.

Synthesis of L-Et. **L-Et** was obtained using the method described for **L-Me** (yellow powder, 2.51 g, 80%). ^{1}H NMR (400 MHz, chloroform-d): δ 7.74 (d, J = 8.2 Hz, 2H), 7.14–6.96 (m, 20H), 6.84 (d, J = 7.0 Hz, 8H), 6.64–6.63 (m, 4H), 6.44 (d, J = 1.9 Hz, 2H), 6.26 (d, J = 7.1 Hz, 2H), 6.00 (t, J = 8.6 Hz, 4H), 5.59 (s, 2H), 5.50 (s, 2H), 2.67 (dq, J = 15.1, 7.5 Hz, 2H), 2.46 (dq, J = 15.0, 7.5 Hz, 2H), 1.21 (t, J = 7.5 Hz, 6H). ^{13}C NMR (101 MHz, chloroform-*d*): δ 161.4, 160.2, 146.8, 140.0, 139.7, 138.7, 137.0, 136.9, 131.2, 130.9, 130.8, 129.8, 128.9, 127.3, 115.2, 54.7, 50.9, 22.7, 13.9. FTIR (KBr, cm^{-1}): 778 (m), 827 (s), 925 (w), 1016 (w), 1095 (w), 1157 (m), 1222 (s), 1450 (w), 1504 (s), 1599 (m), 1658 (ν(C=N), w), 2877 (w), 3052 (w). Anal. calcd for $C_{80}H_{56}F_8N_2$ (1197.33): C, 80.25; H, 4.71; N, 2.34. Found: C, 79.98; H, 4.78; N, 2.31. MS-ESI (*m*/*z*): calcd for $[(C_{80}H_{56}F_8N_2) + H]^+$: 1197.43885. Found: 1197.43610.

Synthesis of L-iPr. **L-iPr** was obtained using the method described for **L-Me** (yellow powder, 1.5 g, 87%). ^{1}H NMR (400 MHz, chloroform-*d*): δ 7.74 (d, J = 8.3 Hz, 2H), 7.13–6.96 (m, 20H), 6.83 (d, J = 7.0 Hz, 8H), 6.61–6.64 (m, 4H), 6.43 (d, J = 2.0 Hz, 2H), 6.22 (d, J = 7.2 Hz, 2H), 6.01 (t, J = 8.6 Hz, 4H), 5.55–5.51 (d, J = 17.8 Hz, 4H), 3.09 (h, J = 6.8 Hz, 2H), 1.24 (d, J = 6.8 Hz, 6H), 1.05 (d, J = 6.9 Hz, 6H). ^{13}C NMR (101 MHz, chloroform-*d*): δ 161.4, 160.2, 146.3, 139.9, 139.7, 139.6, 137.0, 130.9, 130.8, 129.9, 125.0, 115.2, 50.9, 28.2, 24.1. FTIR (KBr, cm^{-1}): 784 (m), 827 (s), 927 (w), 1015 (w), 1092 (w), 1224 (s), 1439 (w), 1462 (w), 1505 (s), 1600 (m), 1667 (ν(C=N), w), 2962 (w). Anal. calcd for $C_{82}H_{60}F_8N_2$ (1225.38) + EtOH: C, 79.35; H, 5.23; N, 2.20. Found: C, 79.71; H, 4.96; N, 2.31. MS-ESI (*m*/*z*): calcd for $[(C_{82}H_{60}F_8N_2) + H]^+$: 1225.47015. Found: 1225.47105.

Synthesis of L-Cl. **L-Cl** was obtained using the method described for **L-Me** (yellow powder, 2.23 g, 77%). ^{1}H NMR (400 MHz, chloroform-d): δ 7.79 (d, J = 8.3 Hz, 2H), 7.21–7.17 (m, 2H), 7.12 (d, J = 1.9 Hz, 2H), 7.07–7.07 (tt, J = 8.7, 4.9 Hz, 16H), 6.89–6.81 (m, 8H), 6.75–6.72 (td, J = 5.5, 2.1 Hz, 4H), 6.57 (d, J = 1.9 Hz, 2H), 6.37 (d, J = 7.1 Hz, 2H), 5.99 (t, J = 8.6 Hz, 4H), 5.63 (s, 2H), 5.48 (s, 2H). ^{13}C NMR (101 MHz, chloroform-d): δ 164.4, 160.4, 145.2, 140.4, 138.9, 137.5, 136.1, 131.3, 130.7, 130.6, 129.4, 129.1, 128.2, 127.1, 122.8, 115.5, 115.3, 54.4, 51.1. FTIR (KBr, cm^{-1}): 731 (w), 776 (m), 823 (s), 896 (w), 1014 (w), 1099 (w), 1158 (m), 1220 (s), 1441 (w), 1505 (s), 1600 (m), 1656 (ν(C=N), w), 1679 (ν(C=N), w), 3062 (w). Anal. calcd for $C_{76}H_{46}Cl_2F_8N_2$ (1210.11): C, 75.43; H, 3.83; N, 2.32. Found: C, 75.29; H, 3.82; N, 2.32. MS-ESI (*m*/*z*): calcd for $[(C_{76}H_{46}Cl_2F_8N_2) + H]^+$: 1209.29831. Found: 1209.29907.

Synthesis of complex

Synthesis of NiBr-Me. A 10 mL solution of dichloromethane was added to a mixture containing the corresponding ligand, **L-Me** (0.25 g, 0.21 mmol), and (DME)$NiBr_2$ (0.063 g, 0.2 mmol). The resulting solution was stirred overnight under a nitrogen atmosphere. After stirring, most of the solvent was removed using a vacuum pump, followed by the addition of diethyl ether to induce complex precipitation. The resulting complex was washed with diethyl ether (3 × 10), filtered, and dried under reduced pressure, resulting in the isolation of the corresponding complex, **NiBr-Me** (red powder, 0.2 g, 72%). FTIR (KBr, cm^{-1}): 718 (w), 778 (m), 827 (s), 958 (w), 1014 (w), 1095 (w), 1156 (m), 1222 (s), 1293 (s), 1505 (s), 1600 (m), 1649 (ν(C=N), w), 3046 (w). Anal. calcd for $C_{78}H_{52}Br_2F_8N_2Ni$ (1387.78) + H_2O: C, 66.64; H, 3.87; N, 1.99. Found: C, 66.57; H, 3.73; N, 2.03. MS-ESI (*m*/*z*): calcd for $[(C_{78}H_{52}F_8N_2)NiBr]^+$: 1305.25341. Found: 1305.25369.

Synthesis of NiBr-Et. **NiBr-Et** was obtained using the method described for **NiBr-Me** (red powder, 0.28 g, 71%). FTIR (KBr, cm^{-1}): 752 (w), 776 (m), 827 (s), 958 (w), 1014 (w), 1097 (w), 1157 (m), 1221 (s), 1294 (w), 1456 (w), 1504 (s), 1601 (m), 1643 (ν(C=N), w), 2973 (w), 3044 (w). Anal. calcd for $C_{80}H_{56}Br_2F_8N_2Ni$ (1415.83) + H_2O: C, 67.01; H, 4.08; N, 1.95. Found: C, 66.82; H, 4.06; N, 1.95. MS-ESI (*m*/*z*): calcd for $[(C_{80}H_{56}F_8N_2)NiBr]^+$: 1333.28471. Found: 1333.28296.

Synthesis of NiBr-iPr. **NiBr-iPr** was obtained using the method described for **NiBr-Me** (red powder, 0.56 g, 89%). FTIR (KBr, cm^{-1}): 777 (m), 829 (s), 957 (w), 1015 (w), 1097 (w), 1157 (m), 1223 (s), 1448 (w), 1504 (s), 1602 (m), 1643 (ν(C=N), w), 2966 (w). Anal. calcd for $C_{82}H_{60}Br_2F_8N_2Ni$ (1443.88) + H_2O: C, 67.37; H, 4.27; N, 1.92. Found: C, 67.04; H, 4.20; N, 1.90. MS-ESI (*m*/*z*): calcd for $[(C_{82}H_{60}F_8N_2)NiBr]^+$: 1361.31601. Found: 1361.31654.

Synthesis of NiBr-Cl. **NiBr-Cl** was obtained using the method described for **NiBr-Me** (red powder, 0.28 g, 98%). FTIR (KBr, cm^{-1}): 774 (m), 831 (s), 897 (w), 954 (w), 1016 (w), 1097 (w), 1157 (m), 1227 (s), 1294 (s), 1447 (w), 1505 (s), 1602 (m), 1652 (ν(C=N), w), 3049 (w). Anal. calcd for $C_{76}H_{46}Br_2Cl_2F_8N_2Ni$ (1336.85) + H_2O·EtOH: C, 62.76; H, 3.65; N, 1.88. Found: C, 62.96; H, 3.77; N, 1.89. MS-ESI (*m*/*z*): calcd for $[(C_{76}H_{46}Cl_2F_8N_2)NiBr + CH_2Cl_2]^+$: 1431.09457. Found: 1431.19537.

Synthesis of NiCl-Me. A 10 mL solution of dichloromethane and 5 mL of ethanol were added to a mixture containing the corresponding ligand, **L-Me** (0.3 g, 0.26 mmol), and $NiCl_2$·$6H_2O$ (0.055 g, 0.23 mmol). The resulting solution was stirred overnight under a nitrogen atmosphere. After stirring, most of the solvent was removed using a vacuum pump, followed by the addition of diethyl ether to induce complex precipitation. The resulting complex was washed with diethyl ether (3 × 10), filtered, and dried under reduced pressure, resulting in the isolation of the corresponding complex, **NiCl-Me** (orange powder, 0.27 g, 91%). FTIR (KBr, cm^{-1}): 718 (w), 775 (m), 827 (s), 1015 (w), 1095 (w), 1156 (m), 1223 (s), 1290 (s), 1505 (s), 1600 (m), 1627 (ν(C=N), w), 1656 (ν(C=N), w), 3051 (w). Anal. calcd for $C_{78}H_{52}Cl_2F_8N_2Ni$ (1316.88) + EtOH: C, 71.44; H, 4.35; N, 2.08. Found: C, 71.58; H, 4.06; N, 2.21. MS-ESI (*m*/*z*): calcd for $[(C_{78}H_{52}F_8N_2)NiCl]^+$: 1261.30393. Found: 1261.30400.

Synthesis of NiCl-Et. NiCl-Et was obtained using the method described for **NiCl-Me** (orange powder, 0.24 g, 80%). FTIR (KBr, cm^{-1}): 778 (m), 827 (s), 926 (w), 1015 (w), 1096 (w), 1157 (m), 1223 (s), 1452 (w), 1505 (s), 1600 (m), 1656 (ν(C═N), w), 2030 (w), 3029 (w). Anal. calcd for $C_{80}H_{56}Cl_2F_8N_2Ni$ (1326.92) + $2H_2O$: C, 70.50; H, 4.44; N, 2.06. Found: C, 70.11; H, 4.45; N, 2.15. MS-ESI (*m*/*z*): calcd for $[(C_{80}H_{56}F_8N_2)NiCl]^+$: 1289.33523. Found: 1289.33551.

Synthesis of NiCl-iPr. NiCl-iPr was obtained using the method described for **NiCl-Me** (orange powder, 0.25 g, 74%). FTIR (KBr, cm^{-1}): 782 (m), 827 (s), 926 (w), 1016 (w), 1095 (w), 1157 (m), 1223 (s), 1441 (w), 1505 (s), 1600 (m), 1660 (ν(C═N), w), 2963 (w). Anal. calcd for $C_{82}H_{60}Cl_2F_8N_2Ni$ (1354.98) + $2H_2O$·EtOH: C, 70.21; H, 4.91; N, 1.95. Found: C, 69.87; H, 4.79; N, 2.18. MS-ESI (*m*/*z*): calcd for $[(C_{82}H_{60}F_8N_2)NiCl]^+$: 1317.36653. Found: 1317.36700.

Synthesis of NiCl-Cl. NiCl-Cl was obtained using the method described for **NiCl-Me** (orange powder, 0.26 g, 79%). FTIR (KBr, cm^{-1}): 736 (w), 775 (m), 825 (s), 897 (w), 930 (w), 1014 (w), 1095 (w), 1157 (m), 1222 (s), 1441 (s), 1505 (s), 1600 (m), 1656 (ν(C═N), w), 3061 (w). Anal. calcd for $C_{76}H_{46}Cl_4F_8N_2Ni$ (1339.70) + EtOH·CH_2Cl_2: C, 64.52; H, 3.70; N, 1.90. Found: C, 64.50; H, 3.90; N, 2.16. MS-ESI (*m*/*z*): calcd for $[(C_{76}H_{46}Cl_2F_8N_2)NiCl + CH_2Cl_2]^+$: 1387.14509. Found: 1387.24438.

Conclusions

In summary, two series of C_2-symmetric nickel complexes were examined in parallel for ethylene polymerization, taking into account steric and electronic factors, as well as the influence of auxiliary ligands. These complexes, all novel, were characterized using a combination of techniques, including single X-ray diffraction analysis. Upon activation with DEAC, these nickel complexes exhibited not only high catalytic activity (up to 12.2 × 10^6 g (PE) mol^{-1} (Ni) h^{-1}) at room temperature but also maintained high activity under industrially relevant conditions (4.8 × 10^6 g (PE) mol^{-1} (Ni) h^{-1}), producing high molecular weight polyethylenes (up to 10^5 g mol^{-1}) with high melt temperatures and controlled branching degrees. Nickel bromide complexes demonstrated significantly higher activities than their chloride counterparts, while exhibiting the opposite trend in terms of polymer molecular weights, underscoring the substantial impact of auxiliary ligands. The sterically hindered nickel bromide complexes were more active than their less hindered counterparts, whereas this trend was reversed for nickel chloride complexes. Moreover, electronic substituents with electron-withdrawing effects were found to decrease the polymerization rate and chain propagation, resulting in semi-crystalline polyethylene with a high melt temperature (134.6 °C) and crystallinity (31.9%). The tailored catalysts, incorporating steric, electronic, and auxiliary ligand modifications, produced thermoplastic polyethylene with impressive combinations of tensile strength (5.9 MPa to 13.9 MPa) and elastic properties (SR = 53% to 81%). These properties render the resulting polyethylene suitable for a wide range of applications requiring high thermal, mechanical, and elastic performance.

Data availability

The data supporting this article have been included as part of the ESI.†

Conflicts of interest

There are no conflicts to declare.

Acknowledgements

This work has been financially supported by the Chemistry and Chemical Engineering Guangdong Laboratory (2111018 and 2132012).

References

1 G. Zanchin and G. Leone, *Prog. Polym. Sci.*, 2021, **113**, 101342.
2 W. A. Braunecker and K. Matyjaszewski, *Prog. Polym. Sci.*, 2007, **32**, 93–146.
3 R. M. Patel, P. Jain, B. Story and S. Chum, *Am. Chem. Soc.*, 2008, **1000**, 71–102.
4 P. D. Hustad, *Science*, 2009, **325**, 704–707.
5 D. J. Arriola, E. M. Carnahan, P. D. Hustad, R. L. Kuhlman and T. T. Wenzel, *Science*, 2006, **312**, 714–719.
6 H. Ohtaki, F. Deplace, G. D. Vo, A. M. LaPointe, F. Shimizu, T. Sugano, E. J. Kramer, G. H. Fredrickson and G. W. Coates, *Macromolecules*, 2015, **48**, 7489–7494.
7 H. Zheng, Y. Li, W. Du, C. S. Cheung, D. Li, H. Gao, H. Deng and H. Gao, *Macromolecules*, 2022, **55**, 3533–3540.
8 (*a*) D. Meinhard, M. Wegner, G. Kipiani, A. Hearley, P. Reuter, S. Fischer, O. Marti and B. Rieger, *J. Am. Chem. Soc.*, 2007, **129**, 9182–9191; (*b*) M. A. Zuideveld, P. Wehrmann, C. Röhr and S. Mecking, *Angew. Chem., Int. Ed.*, 2004, **43**, 869–873.
9 (*a*) Y. Zhang, Y. Zhang, X. Hu, C. Wang and Z. Jian, *ACS Catal.*, 2022, **12**, 14304–14320; (*b*) P. Kenyon, M. Wörner and S. Mecking, Controlled Polymerization in Polar Solvents to UltrahighMolecular Weight Polyethylene, *J. Am. Chem. Soc.*, 2018, **140**, 6685–6689.
10 (*a*) Q. Mahmood and W.-H. Sun, *R. Soc. Open Sci.*, 2018, **5**, 180367; (*b*) H. Liu, W. Zhao, J. Yu, W. Yang, X. Hao, C. Redshaw, L. Chen and W.-H. Sun, *Catal. Sci. Technol.*, 2012, **2**, 415–422; (*c*) J. Lai, X. Hou, Y. Liu, C. Redshaw and W.-H. Sun, *J. Organomet. Chem.*, 2012, **702**, 52–58; (*d*) S. Kong, K. Song, T. Liang, C. Guo, W.-H. Sun and C. Redshaw, *Dalton Trans.*, 2013, **42**, 9176–9187; (*e*) R. Gao, W.-H. Sun and C. Redshaw, *Catal. Sci. Technol.*, 2013, **3**, 1172–1179; (*f*) D. Jia, W. Zhang, W. Liu, L. Wang,

C. Redshaw and W.-H. Sun, *Catal. Sci. Technol.*, 2013, **3**, 2737–2745; (*g*) S. Wang, W.-H. Sun and C. Redshaw, *J. Organomet. Chem.*, 2014, **751**, 717–741; (*h*) X. Ma, X. Hu, Y. Zhang, H. Mu, L. Cui and Z. Jian, *Polym. Chem.*, 2019, **10**, 2596–2607; (*i*) F. Wang and C. Chen, *Polym. Chem.*, 2019, **10**, 2354–2369; (*j*) N. E. Mitchell and B. K. Long, *Polym. Int.*, 2019, **68**, 14–26.

11 Q. Mahmood, Y. Zeng, E. Yue, G. A. Solan, T. Liang and W.-H. Sun, *Polym. Chem.*, 2017, **8**, 6416–6430.

12 K. Lian, Y. Zhu, W. Li, S. Dai and C. Chen, *Macromolecules*, 2017, **50**, 6074–6080.

13 Z. Guan, P. M. Cotts, E. F. McCord and S. J. McLain, *Science*, 1999, **283**, 2059–2062.

14 Z. Hai, Z. Lu, S. Li, Z.-Y. Cao and S. Dai, *Polym. Chem.*, 2021, **12**, 4643–4653.

15 J. M. Eagan, O. Padilla-Vélez, K. S. O'Connor, S. N. MacMillan, A. M. LaPointe and G. W. Coates, *Organometallics*, 2022, **41**, 3411–3418.

16 R. Wu, Y. Wang, R. Zhang, C.-Y. Guo, Z. Flisak, Y. Sun and W.-H. Sun, *Polymer*, 2018, **153**, 574–586.

17 X. Wang, L. Fan, Y. Ma, C.-Y. Guo, G. A. Solan, Y. Sun and W.-H. Sun, *Polym. Chem.*, 2017, **8**, 2785–2795.

18 Q. Zhang, R. Zhang, Y. Ma, G. A. Solan, T. Liang and W.-H. Sun, *Appl. Catal., A*, 2019, **573**, 73–86.

19 R. Wu, Y. Wang, L. Guo, C.-Y. Guo, T. Liang and W.-H. Sun, *J. Polym. Sci., Part A: Polym. Chem.*, 2019, **57**, 130–145.

20 Y. Wang, A. Vignesh, M. Qu, Z. Wang, Y. Sun and W.-H. Sun, *Eur. Polym. J.*, 2019, **117**, 254–271.

21 L. Guo, K. Lian, W. Kong, S. Xu, G. Jiang and S. Dai, *Organometallics*, 2018, **37**, 2442–2449.

22 L.-D. Qin, X.-Y. Wang, Q. Mahmood, Z.-X. Yu, Y.-Z. Wang, S. Zou, T.-L. Liang and W.-H. Sun, *Chin. J. Polym. Sci.*, 2024, **42**, 620–635.

23 H. Saeed, Q. Mahmood, R. Yuan, Y. Wang, S. Zou, K. F. Tahir, Y. Ma, T. Liang and W.-H. Sun, *Polym. Chem.*, 2024, **15**, 1437–1452.

24 J. Fang, X. Sui, Y. Li and C. Chen, *Polym. Chem.*, 2018, **9**, 4143–4149.

25 L. Guo, W. Sun, S. Li, G. Xu and S. Dai, *Polym. Chem.*, 2019, **10**, 4866–4871.

26 Y.-Y. Wang, C.-Q. Wang, X.-Q. Hu, Y. Xia, Y. Chi, Y.-X. Zhang and Z.-B. Jian, *Chin. J. Polym. Sci.*, 2021, **39**, 984–993.

27 X. Ma, Y. Zhang and Z. Jian, *Polym. Chem.*, 2021, **12**, 1236–1243.

28 L. Wang, M. Liu, Q. Mahmood, S. Yuan, X. Li, L. Qin, S. Zou, T. Liang and W.-H. Sun, *Eur. Polym. J.*, 2023, **194**, 112112.

29 X. Li, L. Qin, Q. Mahmood, Z. Yu, S. Zou, Y. Wang, T. Liang and W.-H. Sun, *Eur. Polym. J.*, 2023, **200**, 112520.

30 X. Wang, L. Qin, Q. Mahmood, S. Yuan, Y. Wang, S. Zou, R. Yuan, T. Liang and W.-H. Sun, *Appl. Organomet. Chem.*, 2024, **38**, e7404.

31 Z. Hu, G. Ren, Q. Mahmood, Z. Yu, Y. Wang, K. F. Tahir, S. Zou, T. Liang and W.-H. Sun, *New J. Chem.*, 2024, **48**, 12174–12187.

32 R. Yuan, Y. Wang, Q. Mahmood, Y. Zeng, L. Qin, S. Zou, T. Liang and W.-H. Sun, *Polymer*, 2024, **293**, 126690.

33 Z. Lu, X. Xu, Y. Luo, S. He, W. Fan and S. Dai, *ACS Catal.*, 2023, **13**, 725–734.

34 (*a*) J. T. Medina, Q. H. Tran, R. P. Hughes, X. Wang, M. Brookhart and O. Daugulis, *J. Am. Chem. Soc.*, 2024, **146**, 15143–15154; (*b*) H. Zheng and H. Gao, *Macromolecules*, 2024, **57**, 6899–6913; (*c*) Z. Cheng, H. Gao, Z. Qiu, H. Zheng, D. Li, L. Jiang and H. Gao, *ACS Catal.*, 2024, **14**(10), 7956–7966; (*d*) H. Zheng, Z. Qiu, H. Gao, D. Li, Z. Cheng, G. Tu and H. Gao, *Macromolecules*, 2024, **57**(11), 5279–5288; (*e*) L. Pei, F. Liu, H. Liao, J. Gao, L. Zhong, H. Gao and Q. Wu, *ACS Catal.*, 2018, **8**(2), 1104–1113; (*f*) Y. Gong, S. Li, C. Tan, W. Kong, G. Xu, S. Zhang, B. Liu and S. Dai, *J. Catal.*, 2019, **378**, 184–191; (*g*) C. Wang, D. Wang, Z. Fu, Y. Qin, Q. Zhang and Z. Fan, *J. Catal.*, 2022, **413**, 311–320; (*h*) A. Zhou, R. Yuan, Q. Mahmood, S. Yuan, Y. Wang, Z. Hu, S. Zou, T. Liang and W.-H. Sun, *Polym. Chem.*, 2024, **15**, 4029–4043.

35 D. Zhang, E. T. Nadres, M. Brookhart and O. Daugulis, *Organometallics*, 2013, **32**, 5136–5143.

36 J. L. Rhinehart, N. E. Mitchell and B. K. Long, *ACS Catal.*, 2014, **4**, 2501–2504.

37 J. L. Rhinehart, L. A. Brown and B. K. Long, *J. Am. Chem. Soc.*, 2013, **135**, 16316–16319.

38 C. G. De Souza, R. F. De Souza and K. Bernardo-Gusmão, *Appl. Catal., A*, 2007, **325**, 87–90.

39 L. C. Simon, R. S. Mauler and R. F. De Souza, *J. Polym. Sci., Part A: Polym. Chem.*, 1999, **37**, 4656–4663.

40 R. S. Mauler, R. F. de Souza, D. V. V. Vesccia and L. C. Simon, *Macromol. Rapid Commun.*, 2000, **21**, 458–463.

41 H. Gao, X. Liu, Y. Tang, J. Pan and Q. Wu, *Polym. Chem.*, 2011, **2**, 1398–1403.

42 Q. Mahmood, E. Yue, J. Guo, W. Zhang, Y. Ma, X. Hao and W.-H. Sun, *Polymer*, 2018, **159**, 124–137.

43 Y. Zeng, Q. Mahmood, Q. Zhang, T. Liang and W.-H. Sun, *Eur. Polym. J.*, 2018, **103**, 342–350.

44 D. P. Gates, S. A. Svejda, E. Oñate, C. M. Killian, L. K. Johnson, P. S. White and M. Brookhart, *Macromolecules*, 2000, **33**, 2320–2334.

45 F.-S. Liu, H.-B. Hu, Y. Xu, L.-H. Guo, S.-B. Zai, K.-M. Song, H.-Y. Gao, L. Zhang, F.-M. Zhu and Q. Wu, *Macromolecules*, 2009, **42**, 7789–7796.

46 I. D'Auria, M. Maggio, G. Guerra and C. Pellecchia, *Macromolecules*, 2017, **50**, 6586–6594.

47 G. Leone, M. Mauri, F. Bertini, M. Canetti, D. Piovani and G. Ricci, *Macromolecules*, 2015, **48**, 1304–1312.

48 Q. Mahmood, Y. Zeng, X. Wang, Y. Sun and W.-H. Sun, *Dalton Trans.*, 2017, **46**, 6934–6947.

49 C. Popeney and Z. Guan, *Organometallics*, 2005, **24**, 1145–1155.

50 W. Zhang, P. M. Waddell, M. A. Tiedemann, C. E. Padilla, J. Mei, L. Chen and B. P. Carrow, *J. Am. Chem. Soc.*, 2018, **140**, 8841–8850.

51 W. Lu, W. Fan and S. Dai, *Inorg. Chem. Front.*, 2023, **10**, 108–117.

52 X. Hu, Y. Zhang, B. Li and Z. Jian, *Chin. J. Chem.*, 2021, **39**, 2829–2836.

53 C. S. Popeney and Z. Guan, *Macromolecules*, 2010, **43**, 4091–4097.
54 C. S. Popeney, A. L. Rheingold and Z. Guan, *Organometallics*, 2009, **28**, 4452–4463.
55 L.-S. Lee, H.-j. Ou and H.-l. Hsu, *Fluid Phase Equilib.*, 2005, **231**, 221–230.
56 (*a*) X. Hu, Y. Zhang, Y. Zhang and Z. Jian, *ChemCatChem*, 2020, **12**, 2497–2505; (*b*) J. X. Gao, B. P. Yang and C. L. Chen, *J. Catal.*, 2019, **369**, 233–238; (*c*) J. Fang, X. L. Sui, Y. G. Li and C. L. Chen, *Polym. Chem.*, 2018, **9**, 4143–4149; (*d*) Q. H. Tran, M. Brookhart and O. Daugulis, *J. Am. Chem. Soc.*, 2020, **142**, 7198–7206.
57 D. H. Camacho and Z. Guan, *Chem. Commun.*, 2010, **46**, 7879–7893.
58 S. A. Svejda, L. K. Johnson and M. Brookhart, *J. Am. Chem. Soc.*, 1999, **121**, 10634–10635.
59 D. J. Tempel, L. K. Johnson, R. L. Huff, P. S. White and M. Brookhart, *J. Am. Chem. Soc.*, 2000, **122**, 6686–6700.
60 H. U. Moritz, *Chem. Eng. Technol.*, 1989, **12**, 71–87.
61 Y. Zeng, Q. Mahmood, X. Hao and W.-H. Sun, *J. Polym. Sci., Part A: Polym. Chem.*, 2017, **55**, 1910–1919.
62 Q. Mahmood, J. Guo, W. Zhang, Y. Ma, T. Liang and W.-H. Sun, *Organometallics*, 2018, **37**, 957–970.
63 L. Zhong, G. Li, G. Liang, H. Gao and Q. Wu, *Macromolecules*, 2017, **50**, 2675–2682.
64 R. Wang, X. Sui, W. Pang and C. Chen, *ChemCatChem*, 2016, **8**, 434–440.
65 Y. Liao, Y. Zhang, L. Cui, H. Mu and Z. Jian, *Organometallics*, 2019, **38**, 2075–2083.
66 K. S. O'Connor, A. Watts, T. Vaidya, A. M. LaPointe, M. A. Hillmyer and G. W. Coates, *Macromolecules*, 2016, **49**, 6743–6751.
67 W. Weng, A. H. Dekmezian, E. J. Markel and D. L. Peters, *US. Pat.*, 2001, 62001184327.
68 G. W. Coates and R. M. Waymouth, *Science*, 1995, **267**, 217–219.